Heliyon 8 (2022) e11573

Contents lists available at ScienceDirect

Heliyon

journal homepage: www.cell.com/heliyon

Research article

Plasma-modified graphitic C_3N_4@Cobalt hydroxide nanowires as a highly efficient electrocatalyst for oxygen evolution reaction

Yongjun Shen [a,b,*,1], Yin Chen [b,1], Shuaikang Fang [b,1], Jae Kwang Park [c], Hao Xu [b]

[a] Research Center of Secondary Resources and Environment, School of Chemical Engineering and Materials, Changzhou Institute of Technology, Changzhou, 213022, China
[b] School of Chemistry and Chemical Engineering, Nantong University, Nantong, 226019, China
[c] Department of Civil and Environmental Engineering, University of Wisconsin–Madison, 1415 Engineering Drive, Madison, WI, 53706, USA

ARTICLE INFO

Keywords:
Plasma-modified
Graphitic carbon nitride
Cobalt hydroxide
Electrocatalysis
Oxygen evolution

ABSTRACT

The key to electrocatalytic water splitting is the discovery of efficient, low-cost electrocatalysts for oxygen evolution reaction (OER). g-C_3N_4@$Co(OH)_2$ + PA/X nanowire materials were prepared by a combined strategy of thermo-hydraulic and DBD plasma modification. The morphological structure of the plasma modification for 60 s was then characterised by SEM and TEM patterns. In alkaline media, the g-C_3N_4@$Co(OH)_2$ catalyst subjected to 60-s plasma treatment had excellent durability and exhibited outstanding electrochemical performance, displaying a low overpotential (329 mV). The number of Co^{3+} active sites, high conductivity, and large surface area of the g-C_3N_4@$Co(OH)_2$ + PA/60s catalyst contribute to the remarkable OER activity. This research offers a novel approach to rationally designing effective electrocatalysts for water splitting.

1. Introduction

Growing energy consumption and emission of various polluting gases have prompted people to explore available clean energy sources. Due to its high purity, no secondary pollution and abundant raw material resources, hydrogen energy has become the most popular energy source at present [1]. In recent years, water electrolysis technology has been recognized for its safe preparation process and stable yield [2]. However, the oxygen evolutionary reaction (OER) involves a complex multi-electron transfer process, resulting in a slow reaction rate [3, 4, 5]. Therefore, developing highly active electrocatalysts to speed up the OER process is critical [6]. It is well known that IrO_2 and RuO_2 are the most efficient OER catalysts. However, these materials are expensive, with low natural abundance and poor stability, which limit their large-scale application [7, 8, 9]. In order to design advanced materials, the development of electrocatalysts based on non-precious metal materials and carbon-based alternatives is a viable path [10].

At present, carbon-based materials have attracted great interest because of their mild preparation conditions, customizable structure and low production cost [11]. Because of its high nitrogen concentration, low cost, great chemical stability, and easily tailorable structure, g-C_3N_4 is a viable choice for adding N to carbon materials [12,13]. However, g-C_3N_4 is typically produced by solid-state calcination at high temperatures, which imparts insufficient electrical conductivity, a small surface area, and poor charge transfer characteristics, all of which may impair its catalytic capabilities [14,15]. Hence, there is a need to synthesize hybrid materials containing g-C_3N_4 that can improve the catalytic activity of g-C_3N_4 for OER [16,17]. Transition metal materials and their layered double hydroxides [18], oxides [19,20], perovskites [21,22], phosphides [23,24], sulfides [25,26], and nitrides [27], have been extensively investigated over the last decades, and many of them exhibit significant electrocatalytic activity toward OER. Co-based catalysts have been chosen over other non-precious transition metal-based catalysts owing to their availability and inexpensive cost. In addition, cobalt oxides and hydroxides have outstanding structural properties, high electrical conductivity, and abundant active sites, which bestow them with excellent catalytic activity [28,29]. Yuan et al.coated N-doped carbon layers on $Co_3(PO_4)_2$ nanoparticles. Due to its unique structure and strong synergistic effect, $Co_3(PO_4)_2$@N–C possesses sufficient active sites and excellent electrical conductivity to exhibit efficient OER activity [30]. Consequently, g-C_3N_4/Co-based hybrid materials obtain the advantages of their respective active sites and develop new Co–N active sites, reducing the reaction energy barrier and improving their OER catalytic performance. Thus, these hybrid materials are outstanding OER catalysts and promising alternatives to noble metal catalysts for electrochemical water splitting. Researchers have extensively studied morphological

* Corresponding author.
E-mail address: shenyj@czu.cn (Y. Shen).
[1] These authors have contributed equally to this work and considered as co-first authors.

https://doi.org/10.1016/j.heliyon.2022.e11573
Received 7 April 2022; Received in revised form 25 August 2022; Accepted 7 November 2022

modification, ion doping, defect engineering, composite engineering, and crystal plane control to increase catalytic performance [31,32]; However, there are only a few papers on the application of plasma technology to electrolysis of water. Plasma treatment catalyst has irreplaceable advantages, it can allows the introduction of numerous oxygen vacancies and generating more active sites without destroying the structure of the material, further improving the catalytic activity and OER performance of the catalyst. In particular, no researchers have used plasma technology to further modify g-C_3N_4@Co (OH) $_2$ nanowires.

In this study, we attempted to generate a catalyst with a unique coating structure (g-C_3N_4@$Co(OH)_2$) for OER by a mild preparation method. In order to obtain the best OER performance of the catalysts, the samples were treated with air plasma for different lengths of time. Plasma treatment can generate more active sites without destroying the structure of the material, and thus, improve the catalytic activity. As expected, the g-C_3N_4@$Co(OH)_2$ NW catalyst subjected to 60-s plasma treatment exhibited excellent OER activity. Therefore, this work provides not only an excellent OER electrocatalyst but also provide a new idea for the design of high-performance materials.

2. Experimental section

2.1. Materials and chemicals

Melamine ($C_3H_6N_6$, 99%), urea (CH_4N_2O, 99%), and cobalt chloride hexahydrate ($CoCl_2{\cdot}6H_2O$, 99.99%) were purchased from Rhawn. Deionized water was used throughout the experiment.

2.2. Synthesis of g-C_3N_4 nanosheets

The crucible containing the appropriate amount of melamine powder was placed in a muffle furnace and the heating speed (2.3 °C min^{-1}) as well as the temperature (550 °C) were adjusted. The product obtained at the end of the reaction was g-C_3N_4.

2.3. Synthesis of g-C_3N_4@$Co(OH)_2$ hybrid NW_S

First, a mixture of aqueous solution containing cobalt chloride hexahydrate (1.428 g), urea (0.36 g) and g-C_3N_4 (0.08 g) was ultrasonicated for 120 min to dissolve it fully. Then, Then, it was poured into the reactor and set the temperature to 100 °C. 720 minutes later, the oven was turned off and waited for it to cool down. The resulting product was centrifuged and dried overnight in an oven.

2.4. Synthesis of g-C_3N_4@$Co(OH)_2$ + plasma hybrid NW_S

The experimental setup mainly consists of a plasma generator and an input power supply. First, 50 mg of g-C_3N_4@$Co(OH)_2$ catalyst was weighed on an electronic analytical balance and dispersed uniformly in a quartz reactor. Then place the quartz reactor between the electrode plates and the wiring screws are adjusted to fix it. Turn the voltage adjustment knob to make the input voltage 70V, and turn the current adjustment knob to make the input current 1 A. When current is applied to the electrode plate, a strong current is generated between the upper and lower electrodes, and the current penetrates the air inside the double-layer quartz glass medium to generate plasma for modification. The sample treatment times (60 s, 90 s and 120 s) were varied to obtain plasma-modified composite catalysts, labeled as g-C_3N_4@$Co(OH)_2$ + PA/X (X = 60s, 90s, 120s). So far, team members have published papers on the use of plasma techniques to degrade different dyes [33,34].

2.5. Characterizations

A Bruker D8 X-ray diffractometer (XRD) was used to analyze the crystalline structure of the materials. The morphology of the samples was observed by field emission scanning electron microscopy (FESEM, ZEISS Gemini SEM 300); the structure and composition of the samples were observed by transmission electron microscopy (TEM, Tecnai G2 F20). The chemical valence was recorded with the aid of a Thermo Kalpha-type X-ray energy spectrometer (XPS).

2.6. Electrochemical measurements

All electrochemical performance testing equipment is the electrochemical workstation of the CHI 660E model. The equipment is equipped with a three-electrode system, using the prepared material as the working electrode (contact area of 1 cm^2), the reference electrode as Ag/AgCl, and the counter electrode as a carbon rod. For the tests, the electrolytic cell was filled with 30 ml of 1 M KOH solution. After starting the equipment, the catalyst was first activated by cyclic voltammogram (CV) until a stable image was obtained. The polarization curve was compensated for 85% iR and then tested at a rate of 0.005 V s^{-1}, and the obtained LSV data were fitted to obtain the Tafel slope. To test the AC impedance, an applied voltage of 1.51 V was applied and the frequency was set from 0.01 to 10^5 Hz. The cyclic voltammetric curve was tested by varying the sweep rate at 1.123–1.323 V to obtain the electrochemical capacitance. Finally, the stability was evaluated by chronoamperometry and 1000 turns CV. In this study, the unit discussed in the results is the potential of reversible hydrogen electrode (RHE).

3. Results and discussion

The preparation process of g-C_3N_4@Co (OH) $_2$ + PA composite is shown in Figure 1. First, melamine served as a source of carbon and nitrogen to form g-C_3N_4 nanosheets at 550 °C. Subsequently, g-C_3N_4@Co $(OH)_2$ nanowires were prepared in an oven. Finally, plasma treatment was conducted for different lengths of time (60, 90, and 120 s). Figure 2a depicts a typical X-ray diffraction (XRD) pattern of the produced catalysts. The distinct peaks at $2\theta = 27.6°$ and 13.0° correspond to (002) and (100) of the graphite-carbon nitride and are consistent with the g-C_3N_4 standard card (JCPDS 87–1526). The formation of (002) crystal planes in g-C_3N_4 is produced by the accumulation of a graphite-like lamellar structure, and (100) is caused by the repeated triazine ring structure [35]. The diffraction peak at $2\theta = 27.6°$ is clear and sharp, suggesting that the g-C_3N_4 crystal form is intact and crystallinity is high. The XRD pattern of g-C_3N_4@$Co(OH)_2$ corresponds to the same standard JCPDS data (JCPDS 38–0547), which is consistent with references [36]. However, owing to the low g-C_3N_4 concentration, only a narrow and weak diffraction peak can be observed. The XRD peaks of the plasma-modified samples were are almost the same as those before plasma treatment, regardless of the plasma treatment time, indicating that the composition of the sample was not damaged after 60 s of plasma bombardment.

The morphologies of all prepared samples were characterized by SEM. Figure 2b shows the structure of pure g-C_3N_4, showing a stacked layered structure with a flat and smooth surface. As shown in Figure 2c, $Co(OH)_2$ presents a uniform linear structure with approximately the same length. Figure 2d shows that the g-C_3N_4@$Co(OH)_2$ sample is a nanowire structure covered by a uniform coating. Decoration with g-C_3N_4 is expected to accelerate electron transport of the catalyst. Additionally, Graphite carbon nitride grows on the surface of $Co(OH)_2$, which increases the ECSA of the composite and promotes the complete contact between the electrolyte and the active substance, thus improving the specific capacitance of the material. After 60 s of plasma treatment (Figure 2e), the morphology of the NWs did not change significantly, and the surface of the NWs remained smooth. This indicates that the short duration of the treatment and low plasma energy are not sufficient to change the morphology. However, as the plasma bombardment became longer, the nanowires moved closer to each other (Figures 2f and 2g). Furthermore, some agglomeration and breakage of the NWs was observed. Thus, prolonged plasma treatment not only changes the position of the NWs but also destroys their surface structure. The element composition of g-C_3N_4@$Co(OH)_2$ + PA/60s composite are shown in

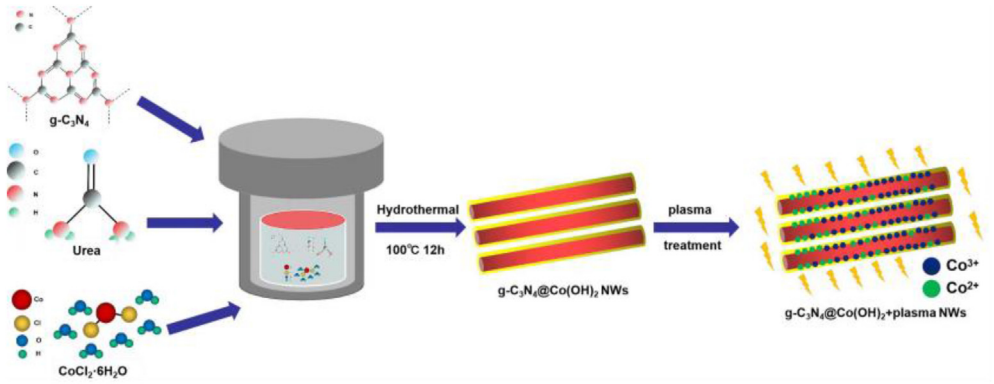

Figure. 1. Schematic illustration of the preparation of the plasma-activated g-C_3N_4@$Co(OH)_2$ hybrid NWs.

Figure 2h. The elements observed in the EDX spectra of the composites are O, Co, C, N, and Cl, which indicated that the catalyst was successfully prepared.

The structures of the g-C_3N_4@$Co(OH)_2$ NWs before and after plasma treatment were investigated using TEM. Figure 3a demonstrates that g-C_3N_4 is composed of ultrathin nanosheets with a layered architecture. As shown in Figure 3b, the surface of $Co(OH)_2$ NWs is uniformly covered with an amorphous layer (g-C_3N_4). After 60 s of plasma treatment (Figures 3c and 3d), the coating of the catalyst was more uniform, and no morphological changes were observed, which is the same as that seen by SEM. This indicates that plasma treatment for 60 s did not damage the crystal structure. We explored the structure and lattice spacing of the material by high-resolution TEM. Figures 3e and 3f demonstrate the presence of a uniform coating of g-C_3N_4. Moreover, the lattice spacing of the catalysts before and after plasma modification is 0.507 nm, corresponding to $2\theta = 17.44°$, which corresponds to the standard card (JCPDS

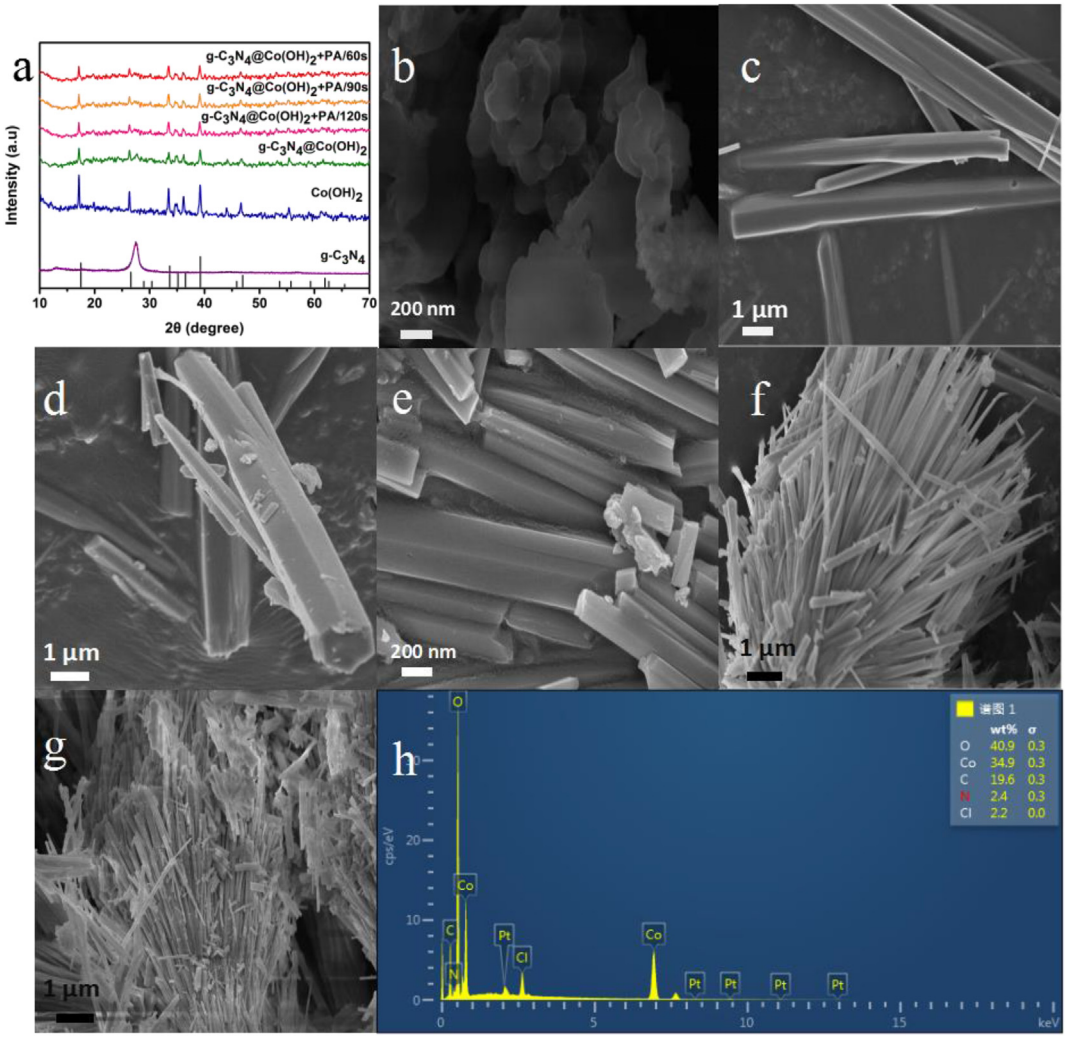

Figure 2. (a) XRD patterns of as-prepared materials. SEM images of (b) g-C_3N_4 nanosheets, (c) $Co(OH)_2$ NWs, (d) g-C_3N_4@$Co(OH)_2$ NWs, (e) g-C_3N_4@$Co(OH)_2$ + PA/60s NWs, (f) g-C_3N_4@$Co(OH)_2$ + PA/90s NWs and (g) g-C_3N_4@ $Co(OH)_2$ + PA/120s NWs. (h) EDX spectrum of g-C_3N_4@$Co(OH)_2$ + PA/60s hybrid NWs.

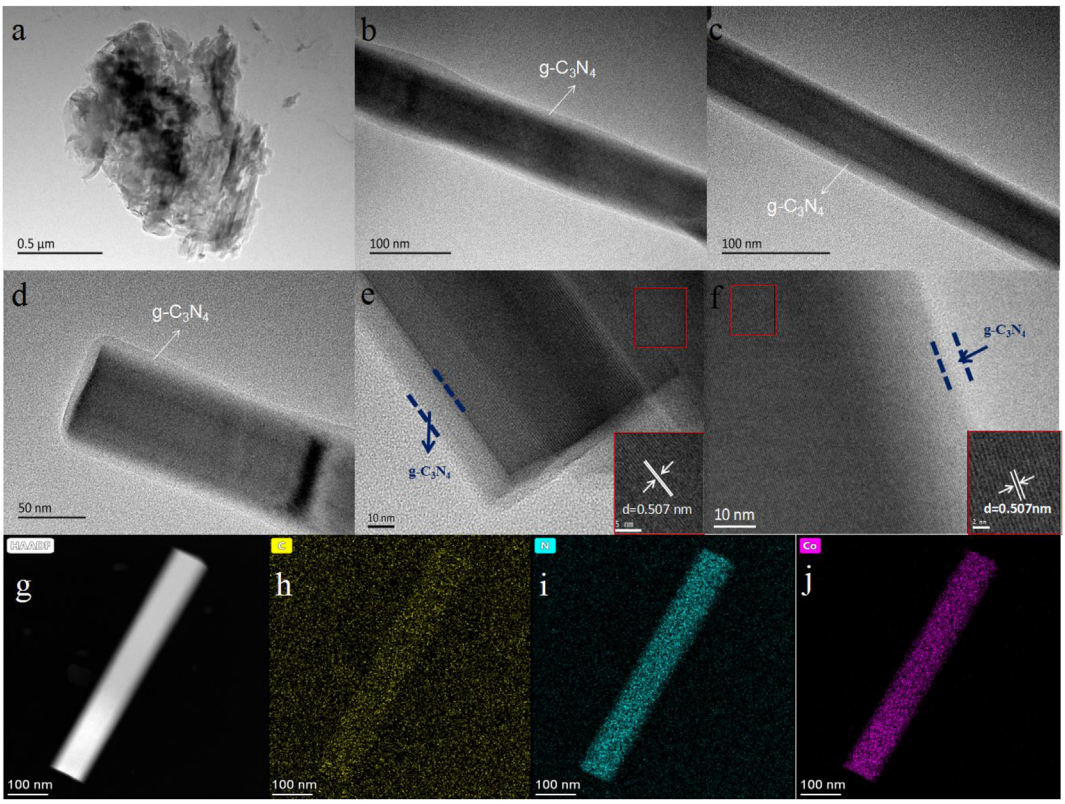

Figure 3. TEM image of (a) g-C_3N_4 nanosheets, (b) g-C_3N_4@$Co(OH)_2$ NWs, (c–d) g-C_3N_4@$Co(OH)_2$ + PA/60s hybrid NWs. (e–f) The high-resolution TEM image of g-C_3N_4@$Co(OH)_2$ and g-C_3N_4@$Co(OH)_2$ + PA/60s hybrid NWs. (g–j) The HADDF image and EDX mapping of C, N and Co from g-C_3N_4@$Co(OH)_2$ + PA/60s hybrid NWs.

38–0547). This indicates that g-C_3N_4@$Co(OH)_2$ NWs exhibit a single crystal structure. In addition, Figures 3g–j are HAADF and EDX images of materials respectively, which clearly show that C, N and Co are uniformly distributed in g-C_3N_4@Co (OH) $_2$ + PA/60s NWs.

We explored the chemical valence states of the materials by XPS characterization technology. The presence of Cl, C, O, N, and Co in the composite was observed from Figure 4a. The C 1s spectrum of the g-C_3N_4 nanosheets was deconvoluted into two peaks (Figure 4b). The two distinct peaks (284.5 eV and 288.1 eV) appearing in the graph are due to the C=C and N–C=N bonds of the triazine ring [37,38]. Compared to Figure 4b, the appearance of additional C–O bonds is observed (Figure 4c). The presence of the C–O peak suggests a synergistic effect between g-C_3N_4 and $Co(OH)_2$. The pyridine-N (397.9 eV), N–C (398.4 eV) and graphite-N (400.0 eV) species correspond to three peaks in the high-resolution N 1s spectrum of g-C_3N_4 (Figure 4d) [39,40]. Figure 4e shows the N 1s spectra of g-C_3N_4@$Co(OH)_2$, in addition to the pyridine-N, N–C and graphitic-N peaks, there is an N–Co bond at 399 eV. The existence of Co–N is again proved the graphitic carbon nitride was successfully coated on cobalt hydroxide nanowires. In addition, the Co–N bond provides enough active sites to make the catalyst have higher catalytic activity and thus accelerate the reaction process [41]. The Co2p XPS spectra of plasma-modified g-C_3N_4@$Co(OH)_2$ (Figure 4g) exhibit the same major peaks as Figure 4f. Figure 4f shows the two main peaks of Co $2p_{3/2}$ and Co $2p_{1/2}$ after fitting. The two main peaks are fitted by Co^{3+} and Co^{2+}, and the colors are the same in the same valence diagram. The two characteristic peaks of Co^{3+} are 780.6eV and 798.6 eV, respectively, while those of Co^{2+} are 782.3 eV and 796.9eV [42,43]. The difference between the two main peaks was greater than 15 eV, which confirms that cobalt is present in multiple oxidation states (Co^{3+} and Co^{2+}) in the g-C_3N_4@$Co(OH)_2$ composites. The peaks located at 786 and 803 eV are satellite peaks of the material. In order to obtain the sample indicating the ratio of Co^{3+} and Co^{2+} atoms, we calculated by the area of the fitting region. The Co^{3+}/Co^{2+} atomic ratio of plasma-modified g-C_3N_4@$Co(OH)_2$ was calculated as 2.60, whereas the Co^{3+}/Co^{2+} atomic ratio of g-C_3N_4@$Co(OH)_2$ was 2.05. The superoxides generated during plasma treatment oxidize Co^{2+} atoms, which leads to an increase in the Co^{3+} content [17]. The research has shown that an increase in Co^{3+} stimulates the transfer rate of charge to the catalyst and offers more electrochemically active site [44,45].

Figure 5 was used to detect the specific surface area of the prepared sample. The Brunauer–Emmett–Teller (BET) specific surfaces areas were 5.6781, 7.5429, 10.8212, and 12.112 $m^2\ g^{-1}$, respectively. Thus, the g-C_3N_4@$Co(OH)_2$ + PA/60s sample has the largest BET specific surface area, providing more electrochemically active sites. In addition, the macroporous structure of the g-C_3N_4@$Co(OH)_2$ + PA/60s hybrid NWs is favorable for electron transfer, which is expected to improve the catalytic activity.

The electrocatalytic properties of all samples were measured by an electrochemical workstation equipped with a three-electrode system. The LSV curves of the catalysts are shown in Figures 6a and 6b. Obviously, the onset potential of g-C_3N_4@$Co(OH)_2$ + PA/60s is lower than that of other catalysts. Similarly, the current density growth rate of g-C_3N_4@$Co(OH)_2$ + PA/60s is higher than that of other catalysts. Furthermore, At the same current value (10 mA cm^{-2}), the g-C_3N_4@$Co(OH)_2$ + PA/60s catalyst exhibits the lowest overpotential (329 mV) compared with g-C_3N_4@$Co(OH)_2$ + PA/90s (367 mV), g-C_3N_4@$Co(OH)_2$ + PA/120s (378 mV), g-C_3N_4@$Co(OH)_2$ (388 mV), $Co(OH)_2$ (426 mV), and g-C_3N_4 (442 mV), which was not even inferior to RuO_2. The reasons for such an excellent electrocatalytic activity may be the following: (1) additional active sites (Co–N, Co^{2+}, and Co^{3+}) are generated by strong coupling interactions generated within the catalyst; (2) the g-C_3N_4 nanosheet coating accelerates the transfer of electrons from the redox site to the electron collector; (3) through plasma treatment for 60 s, the obtained catalyst gains additional Co^{3+} species,

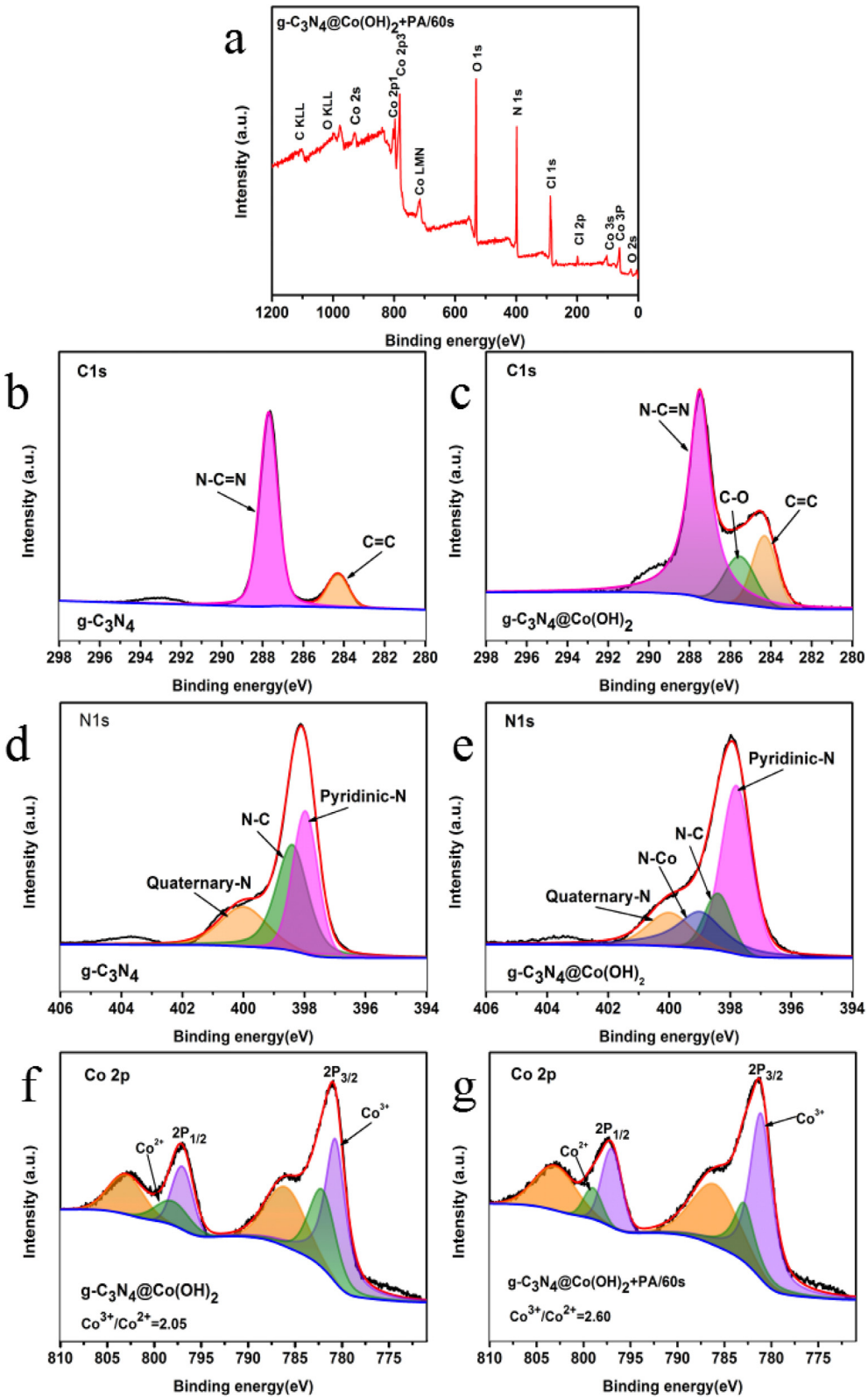

Figure 4. (a) XPS survey spectra of g-C_3N_4@$Co(OH)_2$ + PA/60s, (b–c) C 1s of g-C_3N_4 and g-C_3N_4@$Co(OH)_2$, (d–e) N 1s of g-C_3N_4@$Co(OH)_2$, (f–g) Co 2P spectra of g-C_3N_4@ $Co(OH)_2$ and g-C_3N_4@$Co(OH)_2$ + PA/60s hybrid NWs

increases the active edge sites, and develops a higher specific surface area. With the increase in plasma treatment time, degradation of some catalytic structures and severe aggregation of catalysts occur, so that insufficient active sites could be obtained weakening the catalyst OER activity.

We compared the overpotential of the g-C_3N_4@$Co(OH)_2$ + PA/60s catalyst to those of related carbon-based materials and cobalt-based composites. Sidhureddy et al. [46] compared the catalytic activity Au-doped $Co(OH)_2$ prepared by an electrochemical method with those of pure $Co(OH)_2$, while Au–$Co(OH)_2$ required only a low overpotential (424

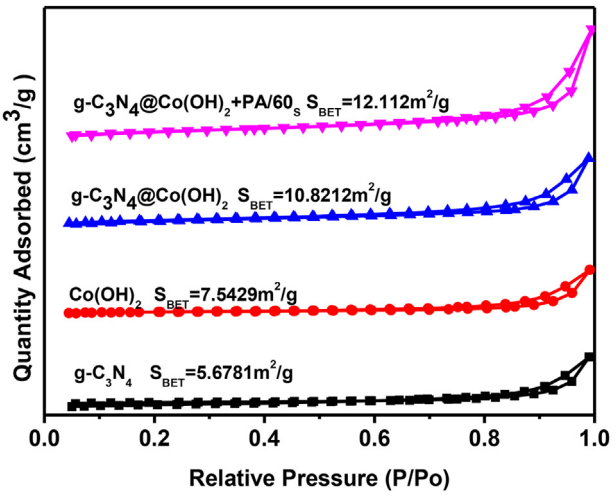

Figure 5. N_2 adsorption-desorption isotherms of g-C_3N_4, $Co(OH)_2$, g-C_3N_4@$Co(OH)_2$, and g-C_3N_4@ $Co(OH)_2$ + PA/60s.

mV) to drive the oxygen evolution reaction. Suliman et al. [47] coupled amorphous CoB nanoparticles with g-C_3N_4 to synthesize CoB/g-C_3N_4 catalysts with excellent OER activity, and CoB/g-C_3N_4 had a lower overpotential (360 mV) compared to CoB and g-C_3N_4 samples. Kumar et al. [48] prepared TC@WO_3@g-C_3N_4@Ni–NiO composites utilizing high temperature hydrolysis and thermal evaporation techniques. The composite has excellent durability and requires only a low overpotential of 385 mV (vs RHE) in the oxygen precipitation reaction. Roy et al. [49] synthesized a $Co(OH)_2$ composite electrocatalyst supported by copper-modified nickel foam with low overpotential and small Tafel slope. Compared with these electrocatalysts, the g-C_3N_4@$Co(OH)_2$ + PA/60s composite has higher OER activity owing to plasma modification.

As shown in Figure 6c, Tafel plots of all modified electrodes were drawn to further understand the OER kinetics. g-C_3N_4@$Co(OH)_2$ + PA/60s exhibits the lowest Tafel slope (199 mV/decade) than that of g-C_3N_4@$Co(OH)_2$ + PA/90s (212 mV/decade), g-C_3N_4@$Co(OH)_2$ + PA/120s (217 mV/decade), g-C_3N_4@$Co(OH)_2$ (230 mV/decade), $Co(OH)_2$ (292 mV/decade), and g-C_3N_4 (302 mV/decade). Sung et al. [50] comprehensively studied the catalytic behavior of a CeO_2/$Co(OH)_2$ hybrid catalyst toward the OER, in which the Tafel slope of $Co(OH)_2$ as a comparative material was 217 mV dec^{-1}. In contrast, the g-C_3N_4@$Co(OH)_2$ + PA/60s catalyst has a lower Tafel slope. C_{dl} of the samples was measured to get an estimate of the ECSA. Figure 6d shows the C_{dl} values of the prepared catalysts. The g-C_3N_4@$Co(OH)_2$ + PA/60s electrode exhibited the largest C_{dl} value (49.9 mF cm^{-2}) compared to the other catalysts, indicating that the composite catalyst with plasma-modified 60s had the highest ECSA. Moreover, the g-C_3N_4@$Co(OH)_2$ + PA/60s catalyst has a higher C_{dl} than other non-noble metal catalysts, For example, Qin et al. synthesized the $Co(OH)_2$-X catalyst by changing the high-temperature etching time of ZIF-67. When the time was 1h, the OER performance was the best, and the C_{dl} of $Co(OH)_2$-1 was 7.5 mF cm^{-2} [51].

The Tafel slope was further analyzed under steady-state conditions. Steady-state polarization curves of the catalysts (Figures 7a–f) were recorded by the current densities after 100 s of chronoamperometric response at different potentials in the catalytic conversion region [52]. The obtained OER steady-state polarization curves were all manually corrected for iR drop (100%) based on the uncompensated resistance. The Tafel plots (Figure 7g) were drawn from the steady-state polarization curves. There is no doubt that at steady state, g-C_3N_4@$Co(OH)_2$ + PA/60s remains the lowest compared to the Tafel values of the other catalysts. The Tafel slope under steady-state conditions again demonstrates the optimal OER activity of the catalyst after 60 s of plasma modification.

We used EIS to further explain the quicker catalytic kinetics of the g-C_3N_4@$Co(OH)_2$ + PA/60s materials. The Nyquist diagram in Figure 8a shows that the R_{CT} of g-C_3N_4@$Co(OH)_2$ + PA/60s (41.2 Ω) is lower than that of other catalysts: g-C_3N_4@$Co(OH)_2$ + PA/90s (55 Ω), g-C_3N_4@$Co(OH)_2$ + PA/120s (58.4 Ω), g-C_3N_4@$Co(OH)_2$ (73.8 Ω), $Co(OH)_2$ (111.2 Ω), and g-C_3N_4 (157.7 Ω). The g-C_3N_4@$Co(OH)_2$ + PA/

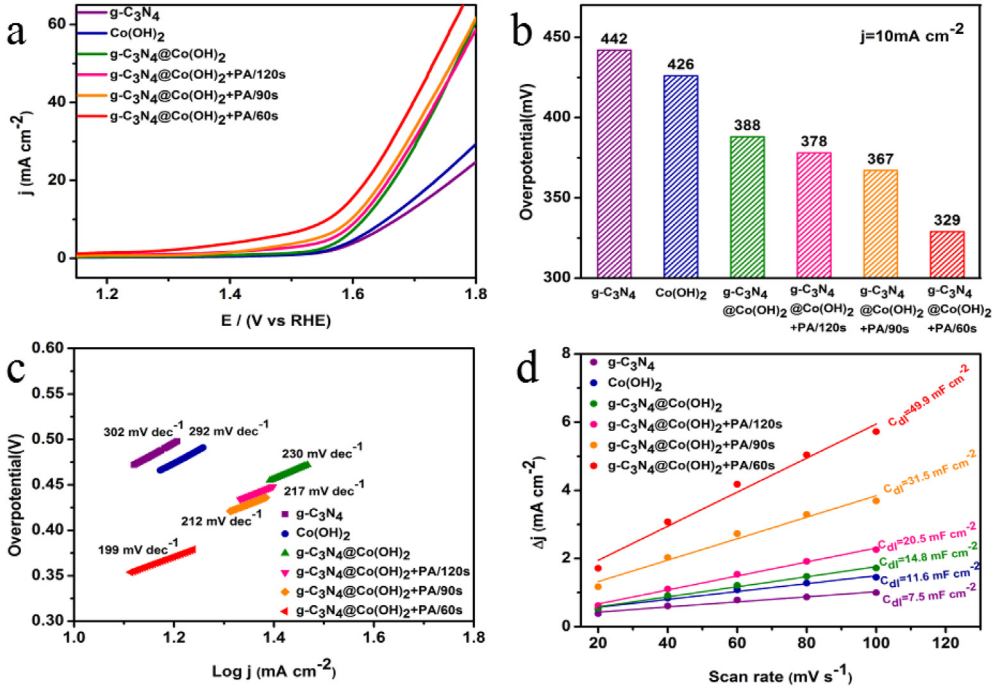

Figure 6. (a) Polarization curves of prepared electrodes in 1M KOH solution. (b) Comparison of overpotentials for various catalysts at current densities of 10 mA cm^{-2} and (c) the Tafel plots. (d) Estimation of Cdl by plotting the current density variation (Δj = (ja− jc)/2).

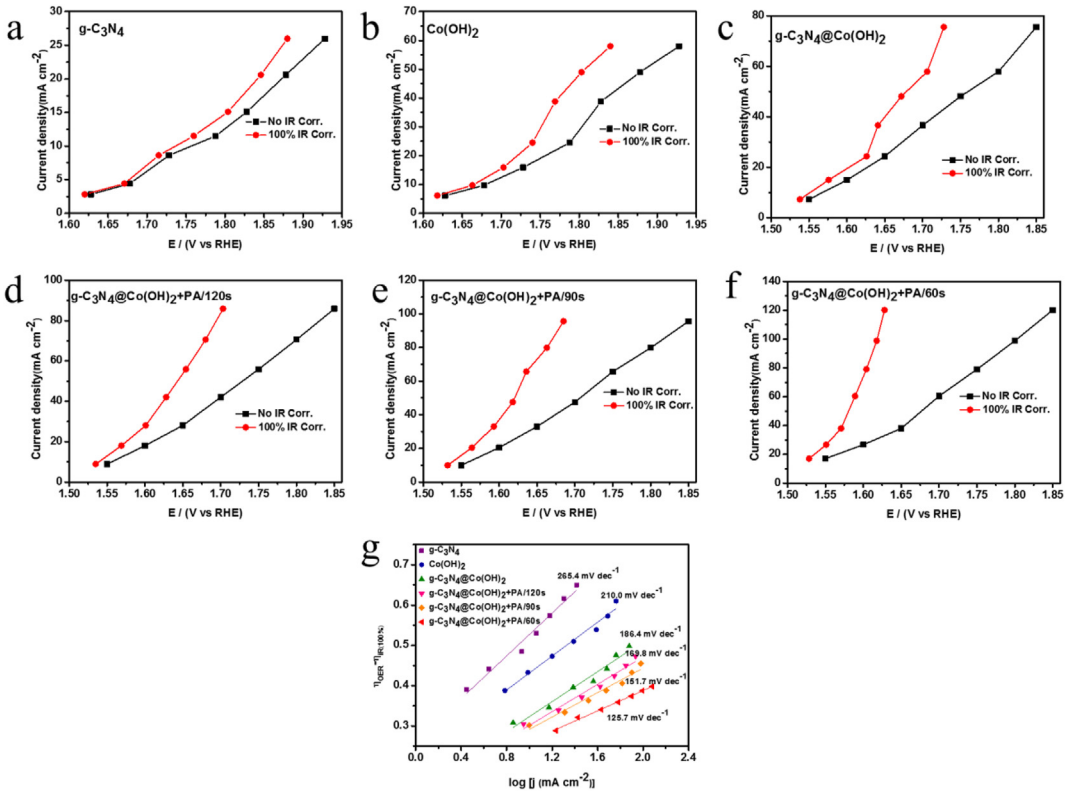

Figure 7. (a–f) OER LSV curves with (red) and without (black) 100% iR drop correction. (g) Corresponding Tafel lines.

60s electrocatalyst had a substantially lower R_{CT} value than the other catalysts. In addition, its R_{CT} value was far inferior to the $Co(OH)_2$ material prepared by Sun et al. [53], which had an R_{CT} value of 150 Ω. In general, fast charge transfer rates can accelerate the combination of electrical integration, and thus, reduce the corresponding ohmic drop [7]. The quantity of active sites in materials increases with the introduction of plasma treatment. To further evaluate the electrochemical stability of g-C_3N_4@$Co(OH)_2$ + PA/60s, a 1000-cycle CV cycling test and a 10-h chronoamperometry test were performed. After the cycling test, the overpotential of g-C_3N_4@$Co(OH)_2$ + PA/60s increased approximately 15 mV at j_{10} (Figure 8b). The inset in Figure 8b shows the time-dependent i-t curve, where the catalyst current remains almost stable at a fixed potential within 10 h. Based on the aforementioned results, the as-prepared g-C_3N_4@$Co(OH)_2$ + PA/60s electrode displays excellent structural stability.

After 10-h chronoamperometry, the g-C_3N_4@$Co(OH)_2$ + PA/60s composites were again characterized by SEM and XPS. It can be clearly seen from Figure 9a that NWs does not change after stability measurement. The XPS (Figure 9b) results show that the Co $2p_{3/2}$ and Co $2p_{1/2}$ peaks are shifted to the right after the OER test (779.5 and 794.6 eV, respectively, compared to 780.9 and 796.8 eV, respectively, for pristine g-C_3N_4@$Co(OH)_2$ + PA/60s). This shift occurs owing to the high oxidation state during chronoamperometry, which results in the formation of CoOOH [54].

Plasma modification improves the catalyst performance because of the following mechanism. First, the quartz reactor is placed between electrodes, and the gas between the electrodes is perforated under high frequency voltage to form many micro-discharge filaments. The electrons in the micro-discharge filaments have a high density and high temperature. When they collide with the molecules and atoms of the discharge gas, they produce a variety of active particles that subsequently react with the catalyst, modifying the material surface. Under the action of air plasma, the catalyst generates more exposed active edge sites and an increased number of Co^{3+} active sites, which accelerate the reaction

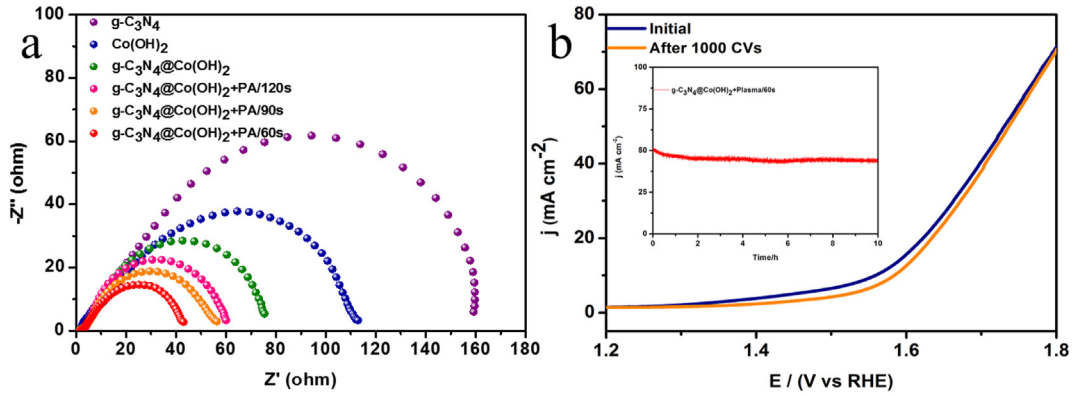

Figure 8. (a) Nyquist plots of various catalysts. (b) OER polarization curves of g-C3N4@ Co(OH)2 + plasma/60s before and after 1000 CV tests.

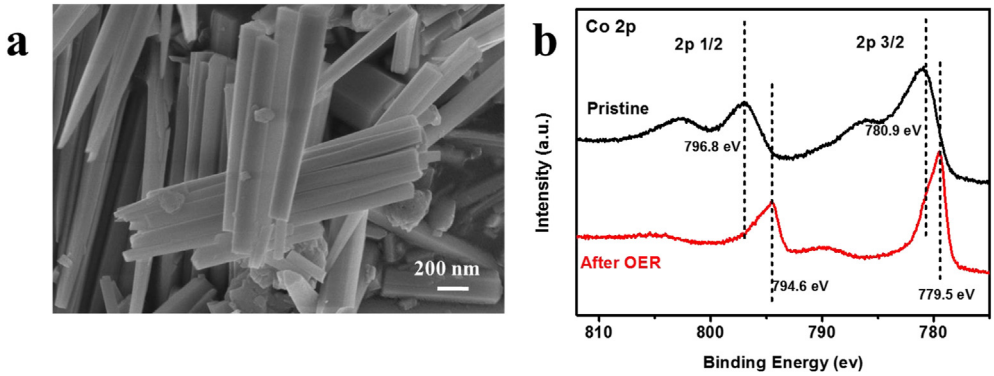

Figure 9. (a) The SEM image and (b) The XPS spectra of g-C_3N_4@$Co(OH)_2$ + PA/60s after 10 h stability measurement in 1 M KOH.

kinetics [55,56]. Plasma modification also provides the g-C_3N_4@$Co(OH)_2$ + PA/60s catalyst with an increased specific surface area and accelerated electron diffusion characteristics [57]. Therefore, plasma technology has strong application potential toward the preparation of advanced catalyst materials.

4. Conclusions

In summary, this study successfully reports on a facile and efficient plasma modification strategy to prepare g-C_3N_4@$Co(OH)_2$ + PA/60s NWs with excellent electrochemical performance. The g-C_3N_4@$Co(OH)_2$ nanowires with a treatment time of 60s had the best catalytic activity at different plasma treatment times, with an overpotential of only 329 mV and the lowest Tafel slope in the oxygen evolution reaction. Furthermore, g-C_3N_4@$Co(OH)_2$ + PA/60s obtained the lowest Tafel slope. XPS tests showed that superoxide in the plasma treatment effectively increased the valence state of Co and thus accelerated the charge transfer rate. In addition, the g-C_3N_4@$Co(OH)_2$ + PA/60s NW catalyst also demonstrated outstanding stability over a 10-h period. The results show that the air plasma modification enables g-C_3N_4@$Co(OH)_2$ + PA/60s to obtain sufficient active sites, good electrical conductivity, and large electrochemical surface area, thereby exhibiting excellent OER activity. This study offers a new direction for the preparation of efficient catalysts to improve the overall OER performance.

Based on the obtained results, the development direction of this work is mainly to prepare composites of g-C_3N_4 with different transition metals, further optimize the plasma modification conditions, improve the plasma modification device, and obtain OER catalysts that are superior to noble metals. In addition, nickel foam, as a three-dimensional structure with high stability superior to carbon paper, can be considered for testing by dropping dispersions onto nickel foam to evaluate the effect of different carriers on catalytic performance. In this paper, the OER performance of catalysts was mainly investigated and the role of plasma on bifunctional catalysts can be continued to be explored. The plasma modification strategy is not only limited to carbon materials and transition metal materials but can also be applied to MOFs-based, non-metallic-based materials, etc., which provides an environmentally friendly and efficient new strategy for designing efficient catalysts.

Declarations

Author contribution statement

Yongjun Shen: Conceived and designed the experiments; Performed the experiments; Analyzed and interpreted the data; Contributed reagents, materials, analysis tools or data; Wrote the paper.

Yin Chen; Shuaikang Fang: Performed the experiments; Analyzed and interpreted the data; Wrote the paper.

Jae Kwang Park: Analyzed and interpreted the data.

Hao Xu: Performed the experiments.

Funding statement

Prof. Yongjun Shen was supported by National Natural Science Foundation of China [21246010], Major Basic Research Project of the Natural Science Foundation of the Jiangsu Higher Education Institutions [22KJA610001], Science and Technology Project Fund of Nantong [JC2021163], Changzhou Institute of technology High-level Talent Research Start-up Project [YN22010].

Data availability statement

Data included in article/supp. material/referenced in article.

Declaration of interest's statement

The authors declare no conflict of interest.

Additional information

No additional information is available for this paper.

References

[1] Z.P. Feng, Y.W. Sui, Z. Sun, J.Q. Qi, F.X. Wei, Y.J. Ren, Z.Z. Zhan, M.H. Zhou, D.M. Meng, L.J. Zhang, L. Ma, Q. Wang, Controllable synthesis of flower-like Mn-Co-P nanosheets as bifunctional electrocatalysts for overall water splitting, Coll. Surf. A Physicochem. Eng. Aspects 615 (2021), 126265.

[2] H.X. Guan, N. Wang, X.X. Feng, S.K. Bian, W. Li, Y. Chen, FeMn bimetallic MOF directly applicable as an efficient electrocatalyst for overall water splitting, Coll. Surf. A Physicochem. Eng. Aspects 624 (2021), 126596.

[3] L. Tian, X.H. Zhai, X. Wang, J. Li, Z. Li, Advances in manganese-based oxides for oxygen evolution reaction, J. Mater. Chem. 8 (2020) 14400–14414.

[4] R. Yoo, K. Min, H. Kim, D. Lim, S.H. Baeck, Prussian blue analog-derived Co/CoTe microcube as a highly efficient and stable electrocatalyst toward oxygen evolution reaction, Appl. Surf. Sci. 581 (2022), 152405.

[5] S. Wang, P. He, L.P. Jia, M.Q. He, T.H. Zhang, F.Q. Dong, M.Z. Liu, H.H. Liu, Y. Zhang, C.X. Li, J. Gao, L. Bian, Nanocoral-like composite of nickel selenide nanoparticles anchored on two-dimensional multi-layered graphitic carbon nitride: a highly efficient electrocatalyst for oxygen evolution reaction, Appl. Catal. B Environ. 243 (2019) 463–469.

[6] S.S. Luo, R. Wang, P. Hei, L.L. Gao, J.Y. Yang, T.F. Jiao, Self-assembled Ni_2P nanosheet – implanted reduced graphene oxide composite as highly efficient electrocatalyst for oxygen evolution reaction, Coll. Surf. A Physicochem. Eng. Aspects 612 (2021), 125992.

[7] L.T. Yan, L. Cao, P.C. Dai, X. Gu, D.D. Liu, L.J. Li, Y. Wang, X.B. Zhao, Metal-organic frameworks derived nanotube of nickel-cobalt bimetal phosphides as highly efficient electrocatalysts for overall water splitting, Adv. Funct. Mater. 27 (2017), 1703455.

[8] Y. Pan, K.A. Sun, S.J. Liu, X. Cao, K.L. Wu, W.-C. Cheong, Z. Chen, Y. Wang, Y. Li, Y.Q. Liu, D.S. Wang, Q. Peng, C. Chen, Y.D. Li, Core-Shell ZIF-8@ZIF-67-derived

CoP nanoparticle -embedded N-Doped carbon nanotube hollow polyhedron for efficient overall water splitting, J. Am. Chem. Soc. 140 (2018) 2610–2618.
[9] Y.K. Zhang, Y. Mo, S. Wang, H. Zhong, Z.F. Cao, X. Ma, Preparation of NiFeCr-based trimetal organic frameworks as electrocatalyst for direct use in oxygen evolution reaction, Coll. Surf. A Physicochem. Eng. Aspects 642 (2022), 128469.
[10] Tian Y. Liang, Y. Li, H. Wang, J. Zhou, J. Wang, T. Regier, H. Dai, Co_3O_4 nanocrystals on graphene as a synergistic catalyst for oxygen reduction reaction, Nat. Mater. 10 (2011) 780–786.
[11] R.G. Zhao, B.X. Ni, L.M. Wu, P.C. Sun, T.H. Chen, Carbon-based iron-cobalt phosphate FeCoP/C as an effective ORR/OER/HER trifunctional electrocatalyst, Coll. Surf. A Physicochem. Eng. Aspects 635 (2022), 128118.
[12] T.Y. Ma, S. Dai, M. Jaroniec, S.Z. Qiao, Graphitic carbon nitride nanosheet-carbon nanotube three-dimensional porous composites as high-performance oxygen evolution electrocatalysts, Angew. Chem. 53 (2014) 7409–7413.
[13] J.Q. Tian, Q. Liu, A.M. Asiri, K.A. Alamry, X.P. Sun, Ultrathin graphitic C_3N_4 nanosheets/graphene composites: efficient organic electrocatalyst for oxygen evolution reaction, ChemSusChem 7 (2014) 2125–2132.
[14] C. Han, Y.D. Wang, Y.P. Lei, B. Wang, N. Wu, Q. Shi, Q. Li, In situ synthesis of graphitic-C_3N_4 nanosheet hybridized N-doped TiO_2 nanofibers for efficient photocatalytic H_2 production and degradation, Nano Res. 8 (2015) 1199–1209.
[15] G.G. Liu, T. Wang, H.B. Zhang, X.G. Meng, D. Hao, K. Chang, P. Li, T. Kako, J.H. Ye, Nature-inspired environmental "phosphorylation" boosts photocatalytic h_2 production over carbon nitride nanosheets under visible-light irradiation, Angew. Chem. Int. Ed. 127 (2015) 13765–13769.
[16] S. Guru, S. Kumar, S. Bellamkonda, R.R. Gangavarapu, Synthesis of CuTi-LDH supported on g-C_3N_4 for electrochemical and photoelectrochemical oxygen evolution reactions, Int. J. Hydrogen Energy 46 (2020) 16414–16430.
[17] L. Xu, Q.Q. Jiang, Z.H. Xiao, X.Y. Li, J. Huo, S.Y. Wang, L.M. Dai, Plasma-engraved Co_3O_4 nanosheets with oxygen vacancies and high surface area for the oxygen evolution reaction, Angew. Chem. Int. Ed. 55 (2016) 5277–5281.
[18] M.Y. Shi, X.C. Sun, Q. Bai, Y. Zhang, S.S. Yu, M.H. Liu, L. Wang, W.W. Yu, N. Sui, Graphdiyne/graphene heterostructure supported NiFe layered double hydroxides for oxygen evolution reaction, Coll. Surf. A Physicochem. Eng. Aspects 637 (2022), 128217.
[19] Y.C. Tan, H.C. Zeng, Self-templating synthesis of hollow spheres of MOFs and their derived nanostructures, Chem. Commun. 52 (2016) 11591–11594.
[20] H. Hu, B. Guan, B. Xia, X.W. Lou, Designed formation of Co_3O_4/$NiCo_2O_4$ double-shelled nanocages with enhanced pseudocapacitive and electrocatalytic properties, J. Am. Chem. Soc. 137 (2015) 5590–5595.
[21] F. Song, K. Schenk, X. Hu, A nanoporous oxygen evolution catalyst synthesized by selective electrochemical etching of perovskite hydroxide $CoSn(OH)_6$ nanocubes, Energy Environ. Sci. 9 (2016) 473–477.
[22] J. Xiong, H. Zhong, J. Li, X.L. Zhang, J.W. Shi, W.W. Cai, K.G. Qu, C.Z. Zhu, Z.H. Yang, S.P. Beckman, H.S. Cheng, Engineering highly active oxygen sites in perovskite oxides for stable and efficient oxygen evolution, Appl. Catal. B Environ. 256 (2019), 117817.
[23] Y.M. Shi, B. Zhang, Recent advances in transition metal phosphide nanomaterials: synthesis and applications in hydrogen evolution reaction, Chem. Soc. Rev. 45 (2016) 1781–1787.
[24] J.Y. Li, M. Zhao, L.Y. Yi, B.M. Feng, C.X. Fang, Z.P. Peng, W.H. Hu, Sacrificial templating synthesis of metal-organic framework hybrid nanosheets as efficient pre-electrocatalyst for oxygen evolution reaction in alkaline, Coll. Surf. A Physicochem. Eng. Aspects 632 (2022), 127745.
[25] W.J. Zhou, X.J. Wu, X.H. Cao, X. Huang, C.L. Tan, J. Tian, H. Liu, J.Y. Wang, H. Zhang, Ni_3S_2 nanorods/Ni foam composite electrode with low overpotential for electrocatalytic oxygen evolution, Energy Environ. Sci. 6 (2013) 2921–2924.
[26] F.S. Khan, M. Sugiyama, K. Fujii, Yu.S. Tver'yanovich, Y. Nakano, Electrochemical reduction of CO_2 using germanium-sulfide-indium amorphous glass structures, Heliyon 6 (2020), e03513.
[27] H.Y. Jin, X. Liu, A. Vasileff, Y. Jiao, Y.Q. Zhao, Y. Zheng, S.Z. Qiao, Single-crystal nitrogen-rich two-dimensional Mo_5N_6 nanosheets for efficient and stable seawater splitting, ACS Nano 1 (2019) 6824–6833.
[28] H.Y. Jin, J. Wang, D.F. Su, Z.Z. Wei, Z.F. Pang, Y. Wang, In situ cobalt-cobalt oxide/N-doped carbon hybrids as superior bifunctional electrocatalysts for hydrogen and oxygen evolution, J. Am. Chem. Soc. 137 (2015) 2688–2694.
[29] A.K. Worku, D.W. Ayele, N.G. Habtu, T.A. Yemata, Engineering Co_3O_4/MnO_2 nanocomposite materials for oxygen reduction electrocatalysis, Heliyon 7 (2021), e08076.
[30] C.Z. Yuan, Y.F. Jiang, Z. Wang, X. Xie, Z.K. Yang, A.B. Yousaf, A.W. Xu, Cobalt phosphate nanoparticles decorated with nitrogen-doped carbon layers as highly active and stable electrocatalysts for the oxygen evolution reaction, J. Mater. Chem. 4 (2016) 8155–8160.
[31] R.R. Zhang, Y.C. Zhang, L. Pan, G.Q. Shen, N. Mahmood, Y.H. Ma, Y. Shi, W. Jia, L. Wang, X. Zhang, W. Xu, J.J. Zou, Engineering cobalt defects in cobalt oxide for highly efficient electrocatalytic oxygen evolution, ACS Catal. 8 (2018) 3803–3811.
[32] K.L. Yan, J.F. Qin, J.H. Lin, B. Dong, J.Q. Chi, Z.Z. Liu, F.N. Dai, Y.M. Chai, C.G. Liu, Probing the active sites of Co_3O_4 for acidic oxygen evolution reaction by modulating Co^{2+}/Co^{3+} ratio, J. Mater. Chem. 6 (2018) 5678–5686.
[33] Y.J. Shen, Y.L. Wang, K.X. Fan, Application of CuO/AC in DBD plasma for dye wastewater treatment: synthesis, optimization, and coupling mechanism, Desalination Water Treat. 138 (2019) 173–182.
[34] Q.H. Xu, S.K. Fang, Y. Chen, J.K. Park, C. Pan, Y.J. Shen, N. Zhu, H.F. Wu, Synergistic photocatalytic activity of a combination of carbon nanotubes-graphene-nickel foam nanocomposites enhanced by dielectric barrier discharge plasma technology for water purification, Water Sci. Technol. 83 (2021) 2762–2777.
[35] Y.Q. Cui, X.Y. Zhang, R. Guo, H.X. Zhanng, B. Li, M.Z. Xie, Q.F. Cheng, X.W. Cheng, Construction of Bi_2O_3/g-C_3N_4 composite photocatalyst and its enhanced visible light photocatalytic performance and mechanism, Separ. Purif. Technol. 203 (2018) 301–309.
[36] M. Tahir, N. Mahmood, L. Pan, Z.F. Huang, Z. Lv, J.W. Zhang, F.K. Butt, G.Q. Shen, X.W. Zhang, S.X. Dou, J.J. Zou, Efficient water oxidation through strongly coupled graphitic C_3N_4 coated cobalt hydroxide nanowires, J. Mater. Chem. 4 (2016) 12940–12946.
[37] Z.H. Pu, I.S. Amiinu, C.T. Zhang, M. Wang, Z.K. Kou, S.C. Mu, Phytic acid-derivative transition metal phosphides encapsulated in N, P-codoped carbon: an efficient and durable hydrogen evolution electrocatalyst in a wide pH range, Nanoscale 8 (2017) 3555–3560.
[38] Y.J. Fu, C.A. Liu, C. Zhu, H.B. Wang, Y.J. Dou, W.L. Shi, M.W. Shao, H. Huang, Y. Liu, Z.H. Kang, High-performance NiO/g-C_3N_4/composites for visible-light-driven photocatalytic overall water splitting, Inorg. Chem. Front. 5 (2018) 1646–1652.
[39] M. Tahir, N. Mahmood, X. Zhang, T. Mahmood, F.K. Butt, I. Aslam, M. Tanveer, F. Idrees, S. Khalid, I. Shakir, Y.M. Yan, J.J. Zou, C.B. Cao, Y.L. Hou, Bifunctional catalysts of Co_3O_4@GCN tubular nanostructured (TNS) hybrids for oxygen and hydrogen evolution reactions, Nano Res. 8 (2015) 3725–3736.
[40] N. Mahmood, M. Tahir, A. Mahmood, J. Zhu, C.B. Cao, Y.L. Hou, Chlorine-doped carbonated cobalt hydroxide for supercapacitors with enormously high pseudocapacitive performance and energy density, Nano Energy 11 (2015) 267–276.
[41] S. Chen, J.J. Duan, M. Jaroniec, S.Z. Qiao, Nitrogen and oxygen dual-doped carbon hydrogel film as a substrate-free electrode for highly efficient oxygen evolution reaction, Adv. Mater. 26 (2014) 2925–2930.
[42] X.H. Luo, Q.L. Zhou, S. Du, J. Li, J.W. Zhong, X.L. Deng, Y.L. Liu, Porous Co_9S_8/nitrogen, sulfur-doped carbon@Mo_2C dual catalyst for efficient water splitting, ACS Appl. Mater. Interfaces 10 (2018) 22291–22302.
[43] X.Q. Ji, R. Zhang, X.F. Shi, A.M. Asiri, B.Z. Zheng, X.P. Sun, Fabrication of hierarchical CoP Nanosheet@Microwire arrays via space-confined phosphidation toward high-efficiency water oxidation electrocatalysis under alkaline conditions, Nanoscale 10 (2018) 7941–7945.
[44] S.W. Li, S.J. Peng, L.S. Huang, X.Q. Cui, A.M. Al-Enizi, G.F. Zheng, Carbon-coated Co^{3+}-Rich cobalt selenide derived from ZIF-67 for efficient electrochemical water oxidation, ACS Appl. Mater. Interfaces 8 (2016) 20534–20539.
[45] L. Qian, Z.Y. Lu, T.H. Xu, X.C. Wu, Y. Tian, Y.P. Li, Z.Y. Huo, X.M. Sun, X. Duan, Trinary layered double hydroxides as high-performance bifunctional materials for oxygen electro-catalysis, ACS Appl. Mater. Interfaces 5 (2015), 1500245.
[46] B. Sidhureddy, A.R. Thiruppathi, A.C. Chen, Au nanoparticle incorporated Co(OH)2 hybrid thin fifilm with high electrocatalytic activity and stability for overall water splitting, J. Electroanal. Chem. 794 (2017) 28–35.
[47] M.A. Suliman, M.H. Suliman, A. Adam, B. Chanbasha, Z.H. Yamani, M. Qamar, Interfacial coupling of amorphous cobalt boride with g-C_3N_4 nanosheets for superior oxygen evolution reaction, Mater. Lett. 268 (2020), 127593.
[48] M.P. Kumar, P. Murugesan, S. Vivek, S. Ravichandran, $NiWO_3$ nanoparticles grown on graphitic carbon nitride (g-C_3N_4) supported toray carbon as an efficient bifunctional electrocatalyst for oxygen and hydrogen evolution reactions, Part. Part. Syst. Char. 34 (2017), 1700043.
[49] A. Roy, K.M. Kang, Y.C. Nah, M. La, D. Choi, S.J. Park, Improved electrocatalytic water oxidation with cobalt hydroxide nano-flflakes supported on copper-modifified nickel foam, Electrochim. Acta 381 (2021), 138368.
[50] M.C. Sung, G.H. Lee, D.W. Kim, CeO2/Co(OH)2 hybrid electrocatalysts for efficient hydrogen and oxygen evolution reaction, J. Alloys Compd. 800 (2019) 450–455.
[51] J.F. Qin, J.Y. Xie, N. Wang, B. Dong, T.S. Chen, Z.Y. Lin, Z.Z. Liu, Y.N. Zhou, M. Yang, Y.M. Chai, Surface Construction of Loose Co(OH)2 Shell Derived from ZIF-67 Nanocube for Efficient Oxygen Evolution, J. Colloid Interface Sci. 562 (2020) 279–286.
[52] S. Anantharaj, S. Noda, M. Driess, P.W. Menezes, The pitfalls of using potentiodynamic polarization curves for tafel analysis in electrocatalytic water splitting, ACS Energy Lett. 6 (2021) 1607–1611.
[53] F.Z. Sun, C.Q. Li, B. Li, Y.Q. Lin, Amorphous mosx developed on $Co(OH)_2$ nanosheets generating efficient oxygen evolution catalyst, J. Mater. Chem. A 5 (2017) 23103–23114.
[54] Q.Z. Qian, Y.P. Li, Y. Liu, G.Q. Zhang, General anion-exchange reaction derived amorphous mixed-metal oxides hollow nanoprisms for highly effifficient water oxidation electrocatalysis, Appl. Catal. B Environ. 266 (2020) 118642.
[55] Y.Q. Yang, H. Mao, R. Ning, X. Zhao, X.H. Zheng, J.H. Sui, W. Cai, Ar plasma-assisted P-doped Ni3S2 with S vacancies for effifffifficient electrocatalytic water splitting, Dalton Trans. 50 (2021) 2007–2013.
[56] M.J. Guo, S.Y. Song, S.S. Zhang, Y. Yan, K. Zhan, J.H. Yang, B. Zhao, Fe-doped Ni-Co phosphide nanoplates with planar defects as an efficient bifunctional electrocatalyst for overall water splitting, ACS Sustain. Chem. Eng. 8 (2020) 7436–7444.
[57] X.S. Liu, P. Liu, F.F. Wang, X.B. Lv, T. Yang, W. Tian, C.H. Wang, S. Tan, J.Y. Ji, Plasma-induced defect engineering and cation refifilling of NiMoO4 parallel arrays for overall water splitting, ACS Appl. Mater. Interfaces 13 (2021) 41545–41554.